Asian Journal of Chemistry; Vol. 38, No. 8 (2026), 2109-2116
ASIAN JOURNAL OF CHEMISTRY
https://doi.org/10.14233/ajchem.2026.36313

Effect of Isolation Techniques on the Structural and Thermal Properties of Nanocellulose: A Comparative Approach

P.H. SAVITHA[1,2], M.S. LATHA[3], H.K. PRADEEP[4], H.S. ONKARAPPA[1] and VIRUPAXAPPA S. BETAGERI[1,*]

[1]Research Centre, Department of Chemistry, GM Institute of Technology (Affiliated to Visvesvaraya Technological University, Belagavi), Davangere-577006, India
[2]Research Centre, Department of Chemistry, GM University, Davanagere-577006, India
[3]Research Centre, Department of Chemistry, Adikavi Sri Maharshi Valmiki University, Raichur-584133, India
[4]Department of Pharmaceutics, GM Institute of Pharmaceutical Sciences and Research, Davanagere-577006, India

*Corresponding author: E-mail: virupaxb@gmail.com

Received: 26 April 2026 *Accepted*: 6 July 2026 *Published online*: 7 August 2026 AJC-22437

Biocompatible materials have attracted considerable interest for the development of bioactive formulations. In this study, nanocellulose was isolated from banana (*Musa acuminata*) rachis using three different approaches *viz*. acid hydrolysis (AH), TEMPO-mediated oxidation (T-cellulose) and ionic liquid treatment (I-cellulose). In acid hydrolysis, the strong acids selectively break the amorphous regions of cellulose by cleaving β-(1→4)-glycosidic bonds, leaving behind highly crystalline nanoscale cellulose particles (nanocellulose). TEMPO mediated process oxidizes surface -OH group into carboxylate groups, while ionic liquid method promotes the fiber swelling and fragmentation. The prepared nanocellulose (NC) was characterised with FTIR spectroscopy, which confirms the presence of cellulose functional groups along with the added carboxylate groups in both samples. XRD analysis revealed well-defined diffraction peaks for TEMPO-treated cellulose, characteristic of a semi-crystalline structure, whereas ionic liquid-treated cellulose exhibited a broader diffraction peak, consistent with a predominantly amorphous structure. SEM and TEM images indicating extended, high-aspect-ratio fibrils in TEMPO cellulose and shorter, uniform fibrils in ionic cellulose, both celluloses forming dense and interconnected structure. TGA and DTA exhibited a three-step decomposition pattern for all samples, with TEMPO-treated cellulose possessing the highest thermal stability.

Keywords: Biodegradable, Nanocellulose, Delignification, Ionic liquid, TEMPO oxidation.

INTRODUCTION

Nanocellulose derived from agricultural byproducts has emerged as a promising sustainable material by integrating biomass valorisation with waste management. Agricultural residues and other lignocellulosic biomass provide abundant, renewable and cost-effective sources for nanocellulose production, supporting the development of eco-friendly sustainable materials [1]. During the past decade, nanocellulose has attracted considerable attention due to its exceptional mechanical strength, biodegradability, high specific surface area and tunable surface chemistry, making it suitable for a wide range of advanced applications [2]. Cellulose, the principal structural polysaccharide of plant cell walls, serves as the primary precursor for nanocellulose production. Agricultural residues such as corn stover, coconut coir, banana rachis, corn stalks and other crop wastes have been successfully converted into value-added nanocellulose, reducing environmental pollution while promoting resource efficiency within a circular bioeconomy [3]. These characteristics have expanded the application of nanocellulose in biodegradable packaging, biomedical devices, construction materials, electronic components and other high-value products [4].

The production of nanocellulose generally involves a series of physico-chemical, mechanical or enzymatic treatments to convert cellulose into nanoscale materials. The initial processing step focuses on the removal of non-cellulosic constituents, primarily lignin and hemicellulose, followed by controlled disintegration of the purified cellulose into nanoscale structures [5]. Depending on the extraction method and the resulting morphology, nanocellulose is commonly classified into cellulose nanocrystals (CNCs), cellulose nanofibrils (CNFs) and bacterial nanocellulose (BNC) [6,7].

CNCs are rod-shaped nanoparticles obtained primarily by acid hydrolysis, which selectively removes the amorphous regions while preserving the crystalline domains of cellulose

This is an open access journal, and articles are distributed under the terms of the Attribution 4.0 International (CC BY 4.0) License. This license lets others distribute, remix, tweak, and build upon your work, even commercially, as long as they credit the author for the original creation. You must give appropriate credit, provide a link to the license, and indicate if changes were made.

[8]. They possess high crystallinity, a large aspect ratio, excellent mechanical strength and abundant hydroxyl groups that facilitate surface functionalisation [9]. These characteristics have led to their use in nanocomposites, packaging, coatings, biomedical devices and electronic materials as a sustainable alternative to synthetic nanomaterials [10,11]. In contrast, CNFs consist of interconnected fibrils containing both crystalline and amorphous regions, with diameters of 5-50 nm and lengths extending to several micrometres [12]. Their high mechanical strength, large surface area, film-forming ability and reactive hydroxyl groups make them suitable for barrier films, hydrogels, coatings, biomedical scaffolds and reinforced polymer composites [13,14]. BNC is synthesised extracellularly by bacteria such as *Gluconacetobacter xylinus* through fermentation and is distinguished by its high purity, crystallinity and 3D nanofibrous network without lignin or hemicellulose, simplifying downstream processing [15-17].

The structure and properties of nanocellulose are governed by the synthesis method. Mechanical approaches such as high-pressure homogenisation, grinding, ultrasonication, cryocrushing and ball milling, primarily produce CNFs by fibrillating cellulose fibres without extensive chemical modification [18-22]. Chemical routes are commonly employed for CNC production and surface functionalisation. Acid hydrolysis selectively removes amorphous cellulose to yield highly crystalline, well-dispersed nanocrystals [23,24]. TEMPO-mediated oxidation converts the primary hydroxyl groups at the C6 position into carboxyl groups under mild alkaline conditions, enhancing surface charge, hydrophilicity, dispersibility and chemical reactivity, making the resulting nanocellulose attractive for membranes, hydrogels, packaging and biomedical applications [25-28]. Ionic liquid (IL) processing has emerged as a greener alternative since ILs efficiently disrupt the hydrogen-bonding network of cellulose under relatively mild conditions, enabling cellulose dissolution, regeneration and subsequent nanocellulose production while offering solvent recyclability and reduced environmental impact [29-33].

The selection of a nanocellulose synthesis route depends on the cellulose source, the desired material properties, production cost and environmental sustainability [34,35]. Since different preparation methods alter crystallinity, surface chemistry and morphology, they can substantially influence the performance of nanocellulose in applications such as nanocomposites, packaging, coatings, membranes and biomedical materials [36-38]. Although several synthesis strategies have been reported, a systematic comparison of nanocellulose derived from the same agricultural feedstock using different preparation methods remains limited.

Banana (*Musa acuminata*) rachis is an abundant agricultural residue and an underutilised source of cellulose for value-added material production. In the present study, nanocellulose was isolated from banana rachis by acid hydrolysis, TEMPO-mediated oxidation and ionic liquid treatment to compare the influence of these synthesis routes on the structural, morphological and thermal characteristics of the resulting materials. The prepared nanocellulose was characterised using FTIR, XRD, SEM, TEM, TGA and DTA to identify the most suitable approach for producing biocompatible nanocellulose for bioactive applications [6].

EXPERIMENTAL

Banana rachis used as the feedstock was collected from fruit vendors and agricultural fields in Davangere, India. Chlorobutane and 1-methylimidazole were obtained from Sigma-Aldrich, while 2,2,6,6-tetramethylpiperidine-1-oxyl (TEMPO), 40% H_2SO_4, NaBr, $NaClO_2$, NaClO, CH_3COOH and 5% NaOH were purchased from SD Fine Chemicals, Mumbai, India. All chemicals were of analytical grade with a minimum purity of 98% and were used as received without further purification to ensure experimental consistency and reproducibility.

Alkali pre-treatment: Banana rachis (10 g) was finely milled and sieved to obtain a uniform particle size. The powdered biomass was treated with 5% NaOH at 85-100 ºC for 2 h to remove surface waxes, pectin and hemicellulose. Following alkali treatment, the fibres were thoroughly washed with deionised water until a neutral pH was achieved, ensuring complete removal of residual alkali. The treated material was then oven-dried for 24 h or until a constant weight was attained, to eliminate residual moisture. This pretreatment increased fibre accessibility and improved the efficiency of the subsequent bleaching and nanocellulose isolation steps.

Fig. 1 illustrates the chemical interaction between cellulose and NaOH during alkali pretreatment. The hydroxyl groups of cellulose react with NaOH to form sodium cellulose (–ONa), accompanied by the release of water. This conversion alters the fibre surface by increasing the density of negatively charged sites without disrupting the cellulose polymer framework. As a result, the treated fibres exhibit enhanced chemical reactivity, facilitating subsequent bleaching, surface modification and efficient nanocellulose extraction.

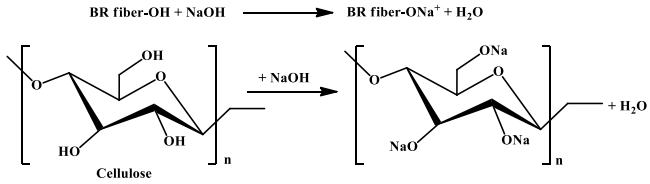

Fig. 1. BR-Alkali treatment with NaOH

Bleaching of alkali residue: The alkali-treated banana rachis was subjected to bleaching to remove residual lignin and enhance fibre whiteness. The dried material was dispersed in deionised water and treated with sodium chlorite ($NaClO_2$) in the presence of acetic acid as a buffering agent. The reaction mixture was maintained at 60 ºC under continuous stirring for 1-2 h to promote selective oxidation of lignin and other coloured impurities. After bleaching, the cellulose-rich fibres were recovered by filtration and thoroughly washed with distilled water until a neutral pH was attained. The bleached fibres were then dried in a hot-air oven at 60 ºC until a constant weight was obtained, producing purified cellulose suitable for subsequent nanocellulose synthesis.

TEMPO catalysed oxidation to bleached cellulose: The bleached cellulose fibres were oxidised using a TEMPO-mediated system to introduce –COOH groups onto the cellulose chains. The fibres were dispersed in deionised water, and

the pH of the suspension was adjusted to 10-11 using dilute NaOH. 2,2,6,6-Tetramethylpiperidine-1-oxyl (TEMPO) was employed as the primary catalyst, while NaBr served as the co-catalyst. The oxidation reaction was initiated by the dropwise addition of NaClO under continuous stirring at room temperature. Throughout the reaction, the pH was continuously monitored and maintained within the desired range by the addition of NaOH to compensate for the OH^- ions consumed during oxidation.

TEMPO-oxidised nanocellulose was prepared by dispersing 1 g of banana rachis cellulose in 100 mL of deionised water. In a separate vessel, 0.06 g of TEMPO and 0.1 g of NaBr were dissolved in 50 mL of deionised water and subsequently added to the cellulose suspension. The oxidation reaction was initiated by the dropwise addition of 10% (w/v) NaClO, while maintaining the pH at approximately 10 by adding NaOH solution dropwise. Upon completion of the reaction, the suspension was quenched with deionised water, and the pH was adjusted to 7 using 0.5 M HCl. The reaction mixture was diluted to a final volume of 200 mL, homogenised at 10,000 rpm, and ultrasonicated for 10 min to promote uniform fibrillation. The resulting TEMPO-oxidised banana rachis nanocellulose (T-cellulose) suspension was thoroughly washed and dried at 40 ºC to remove residual reagents, yielding approximately 95% nanocellulose.

Fig. 2 illustrates the TEMPO-mediated oxidation mechanism, in which the primary hydroxyl groups at the C6 position of cellulose are selectively converted first into aldehyde inter-mediates and subsequently into carboxyl groups. This selective surface modification enhances the hydrophilicity and aqueous dispersibility of cellulose while introducing reactive functional groups for further chemical modification. The cellulose backbone remains intact throughout the oxidation process, producing highly functionalised nanocellulose suitable for advanced biomedical and material applications.

Ionic liquid (IL) method: In this study, 1-butyl-3-methylimidazolium chloride ([BMIM]Cl) was selected due to its ability to disrupt the strong intermolecular hydrogen-bonding network within cellulose, as illustrated in Fig. 3. In brief, banana rachis nanocellulose was synthesised by adding 10 g of [BMIM]Cl to a 100 mL three-neck round-bottom flask fitted with a condenser and heated in an oil bath. After complete melting of the ionic liquid, 1 g of purified banana rachis cellulose was gradually introduced under continuous magnetic stirring and the reaction mixture was maintained at 120-125 ºC for 1 h. Formation of a light-yellow homogeneous solution indicated effective dissolution of cellulose in the ionic liquid medium [40]. The reaction was terminated by the gradual addition of 50 mL of cold deionised water under continuous stirring, resulting in the regeneration and precipitation of nanocellulose. The precipitated material was filtered and washed 5-6 times with cold deionised water to remove residual ionic liquid. The purified banana rachis nanocellulose (I-cellulose) was then collected, dried and stored (yield: 92%).

Characterisation: The structural, chemical, morphological and thermal properties of cellulose extracted from banana rachis and the prepared nanocellulose samples (T-cellulose and I-cellulose) were characterised using various analytical techniques. Functional groups were analysed by FTIR (Bruker ALPHA II, ATR mode) over the range of 4000-400 cm^{-1}. Crystalline structure was examined using a Bruker D8 Advance X-ray diffractometer with Cu*K*α radiation to evaluate crystallinity and phase characteristics. Thermal behaviour was investigated using a NETZSCH STA 2500 thermal analyser by recording TGA and DTA curves from 25 to 800 ºC at a heating rate of 5 ºC min^{-1} under a nitrogen atmosphere. Surface morphology was examined using a TESCAN VEGA3 scanning electron microscope (SEM) operated at an accelerating voltage of 25 kV, while particle size and nanostructure were further analysed by transmission electron microscopy (TEM) at an accelerating voltage of 120 kV using well-dispersed samples.

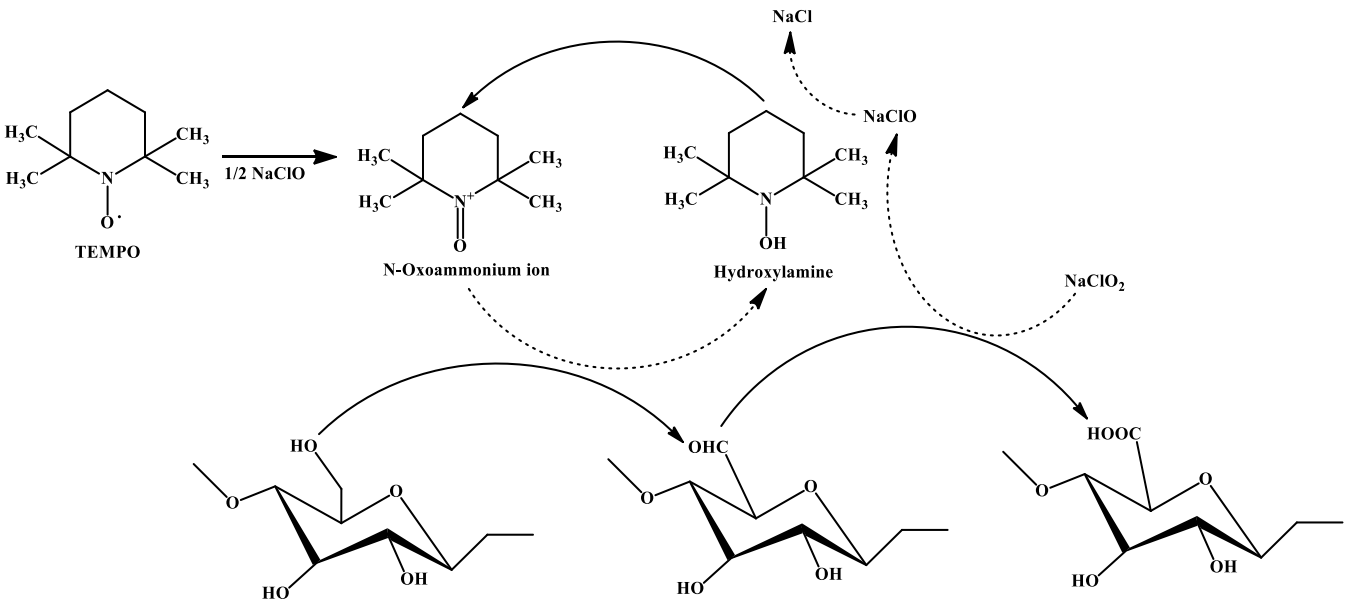

Fig. 2. TEMPO mediated oxidation mechanism [39]

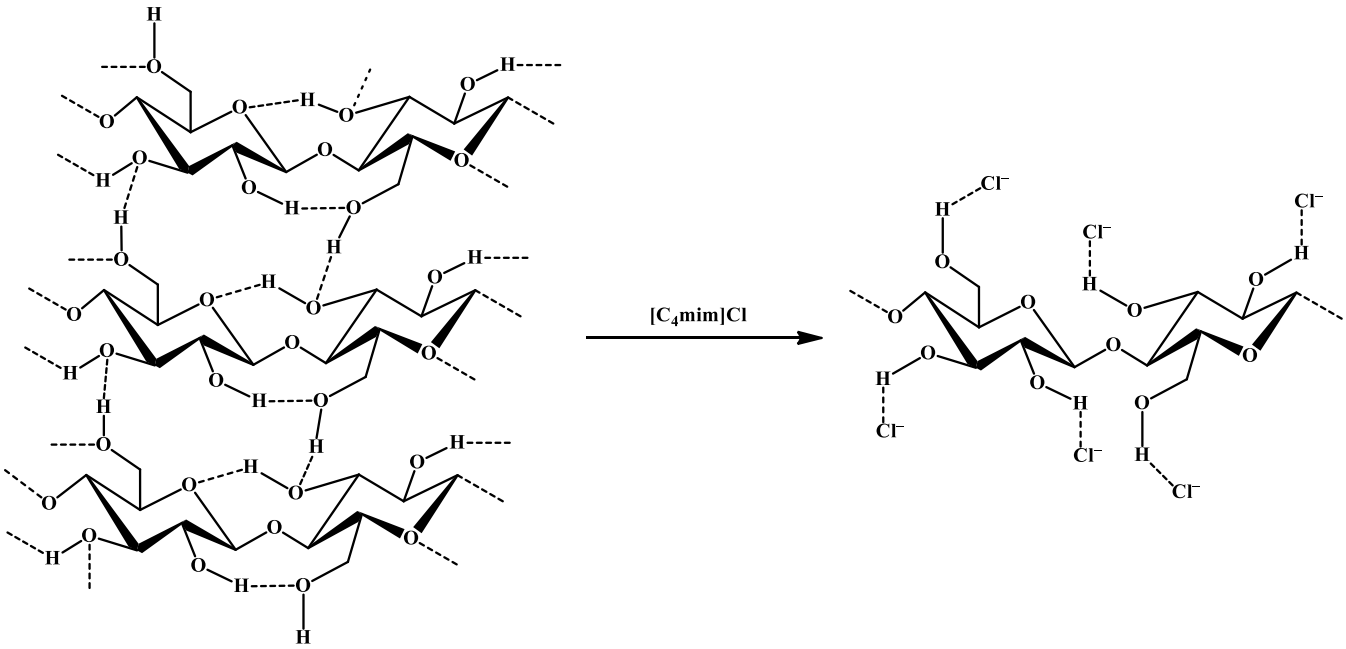

Fig. 3. Mechanistic representation of cellulose–ionic liquid interactions [6]

RESULTS AND DISCUSSION

FTIR studies: The FTIR spectra of cellulose, ionic cellulose and TEMPO-oxidized cellulose are shown in Fig. 4a, with the enlarged fingerprint region shown in Fig. 4b. All samples exhibited a broad absorption band between 3326 and 3344 cm^{-1}, corresponding to O–H stretching vibrations, which confirms the polysaccharide structure of cellulose and the presence of extensive intermolecular hydrogen bonding. The absorption band at 1657-1629 cm^{-1} is assigned primarily to the H–O–H bending vibration of absorbed water and hydrogen-bonding interactions within the cellulose network. Ionic cellulose exhibited distinct absorption bands at 1495.74 and 1343.70 cm^{-1}, which are assigned to CH_2 and C–H bending vibrations. These changes suggest rearrangement of the cellulose structure after ionic liquid treatment. Absorption bands between 1206 and 1147 cm^{-1} arise from asymmetric C–O–C stretching, whereas bands in the range of 1182-1096 cm^{-1} are attributed to C–O–C and C–O stretching vibrations of the cellulose backbone and β-(1→4)-glycosidic linkages. The band located between 1054 and 1032 cm^{-1} is characteristic of the pyranose ring and remained present after chemical treatment. A band at 911 cm^{-1} was detected in TEMPO-oxidized cellulose, while ionic cellulose displayed a band at 863.71 cm^{-1}, both characteristic of β-glycosidic skeletal vibrations. The additional absorption band at 717.63 cm^{-1} in ionic cellulose is related to changes in the crystalline arrangement of regenerated cellulose. Although slight shifts in peak positions were observed after ionic liquid treatment and TEMPO oxidation, the characteristic absorption bands of cellulose remained unchanged,

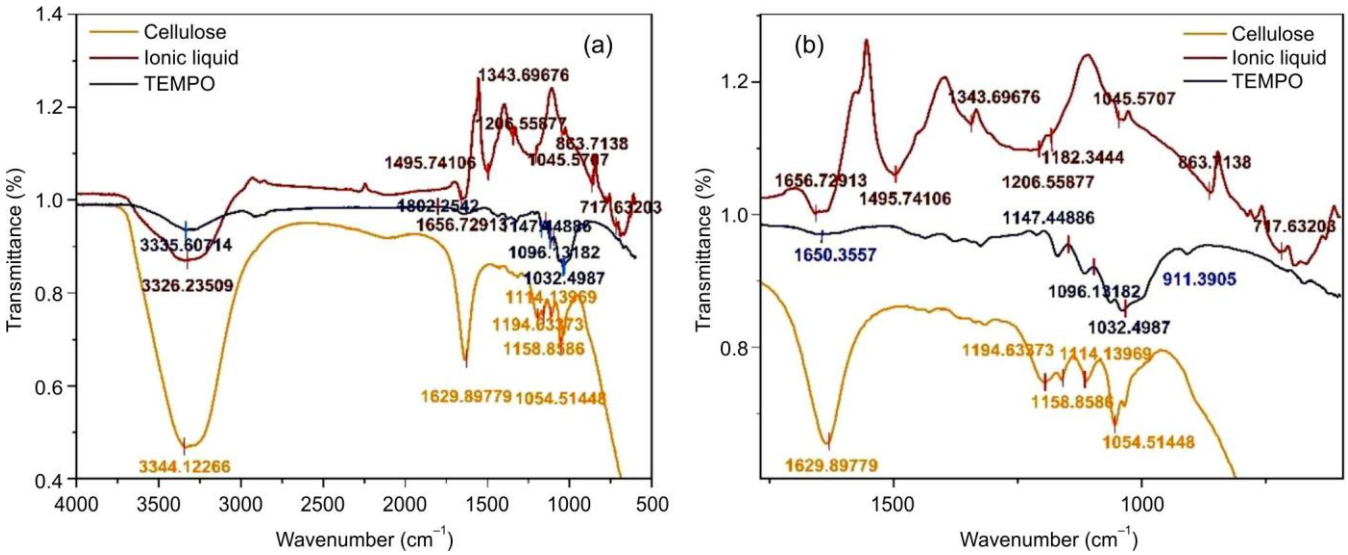

Fig. 4. FTIR (a) and Expanded FTIR (b) spectra (1800-500 cm^{-1}) of cellulose, ionic cellulose and TEMPO-oxidized cellulose

confirmed that the primary cellulose framework was preserved while the chemical treatments modified the hydrogen-bonding network.

XRD studies: The XRD patterns of cellulose (C), ionic cellulose (IC) and TEMPO-oxidized cellulose (TC) are shown in Fig. 5 and the crystallographic parameters are summarized in Table-1. Native cellulose showed characteristic diffraction peaks at 15.69º and 22.92º, which are typical of the cellulose I crystalline structure. Following ionic liquid treatment, new diffraction peaks appeared at 12.47º, 29.04º and 43.48º, accompanied by changes in peak intensity and position. These changes are consistent with rearrangement of the cellulose chains during dissolution and regeneration. TEMPO-oxidized cellulose displayed diffraction peaks at 13.39º, 28.71º and 42.33º, with only small differences in peak positions compared with ionic cellulose. The crystallite sizes calculated using the Scherrer equation were 68.74 nm for cellulose, 85.99 nm for ionic cellulose and 83.80 nm for TEMPO-oxidized cellulose. The corresponding crystallinity indices were 87.04%, 95.24% and 90.96%, respectively. Both chemical treatments increased the crystallite size and crystallinity relative to native cellulose. This behaviour may be related to rearrangement of the cellulose chains together with partial removal of amorphous regions during treatment, giving rise to larger crystalline domains.

TABLE-1
XRD RESULTS OF CELLULOSE, IONIC CELLULOSE AND TEMPO-OXIDISED CELLULOSE

Cellulose type	Main peak (2θ)	Crystallite size (nm)	Crystallinity index (%)
C	22.92	68.74	87.04
IC	29.04	85.99	95.24
TC	28.71	83.80	90.96

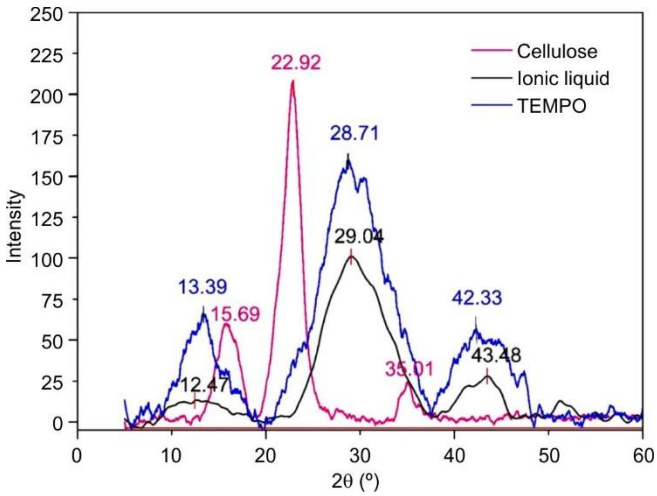

Fig. 5. XRD patterns of cellulose, ionic cellulose and TEMPO cellulose

Thermal studies: The TG curves of ionic liquid-treated nanocellulose and TEMPO-oxidized nanocellulose were measured over the temperature range of 30-490 ºC to evaluate their thermal degradation behaviour (Fig. 6a). Both samples underwent multistep weight loss during heating. The initial weight loss below 100 ºC is attributed to the evaporation of physically adsorbed moisture and residual volatile components. Between 100 and 220 ºC, only a small decrease in mass was recorded and both materials remained relatively stable throughout this temperature range.

The major degradation stage occurred between 220 and 350 ºC and is associated with the cleavage of β-(1→4)-glycosidic linkages, depolymerization and decomposition of the cellulose backbone. Ionic nanocellulose showed a rapid weight loss in this region, whereas TEMPO-oxidized nanocellulose degraded over a broader temperature range. Above 350 ºC, both samples underwent further mass loss owing to the decomposition of carbonaceous residues. At 490 ºC, the residual mass of TEMPO-oxidized nanocellulose was approximately 35%, whereas ionic nanocellulose retained about 17%. The higher char residue of the TEMPO sample may be related to the presence of oxygen-containing functional groups introduced during TEMPO oxidation. These results confirmed that TEMPO oxidation improved char formation and thermal stability compared with ionic liquid-treated nanocellulose.

The DT curves of ionic liquid-treated nanocellulose and TEMPO-oxidized nanocellulose are shown in Fig. 6b. The

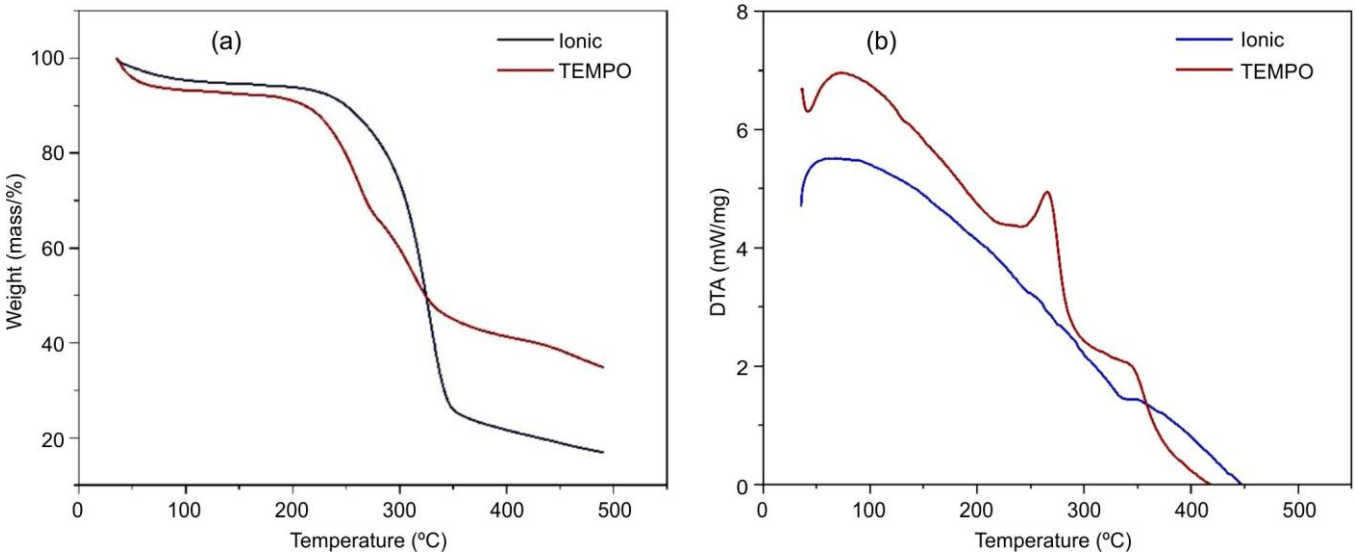

Fig. 6. TGA (a) and DTA (b) curves of I-cellulose and T-cellulose

analysis was carried out over the temperature range of 30-450 ºC to examine the thermal transitions of both materials. Below 100 ºC, a weak thermal event was observed for both samples and is attributed to the removal of physically adsorbed moisture. The TEMPO-oxidized nanocellulose sample exhibited a higher DTA response than ionic nanocellulose in this region, which may be related to stronger interactions between cellulose chains and oxygen-containing functional groups.

Between 100 and 250 ºC, the DTA signal decreased gradually for both samples, corresponding to the onset of thermal degradation of cellulose. An additional thermal occurrence appeared at approximately 260-280 ºC in the TEMPO sample and may be associated with the decomposition of oxygen containing functional groups introduced during oxidation. Above 300 ºC, the DTA signal continued to decrease as decomposition of the cellulose backbone progressed. Thermal decomposition of the TEMPO sample was completed at ~420 ºC, whereas ionic nanocellulose reached completion at about 450 ºC. The difference in the thermal profiles reflects the influence of TEMPO oxidation on the degradation behaviour of nanocellulose while remaining consistent with the patterns observed in the TG analysis.

SEM studies: The SEM micrographs of ionic liquid-treated nanocellulose are shown in Fig. 7a-c. The samples exhibited a porous and interconnected network composed of fibrillar structures with irregular morphology. Ionic liquid treatment promoted defibrillation of the cellulose fibres, producing slender ribbon-like fibrils with widths of ~20-200 nm and lengths extending to several micrometres. During drying, these fibrils became closely packed and formed compact film-like aggregates, a characteristic feature commonly observed in nanocellulose materials. The fibrillar morphology demonstrates effective disintegration of the cellulose fibres into nanoscale structures.

The SEM images of TEMPO-oxidized nanocellulose shown in Fig. 7d-f exhibited a denser and more homogeneous fibrillar network than ionic liquid-treated nanocellulose. The fibrils were more uniformly distributed and appeared as interconnected high-aspect-ratio structures with reduced aggregation. The compact morphology is consistent with the structural modification introduced during TEMPO oxidation and agrees with the FTIR and XRD results.

A comparison of the two samples showed that both ionic liquid treatment and TEMPO oxidation facilitated the nanofibrillation of cellulose. TEMPO-oxidized nanocellulose possessed a denser and more interconnected fibrillar network than ionic liquid-treated nanocellulose, making it more suitable for applications such as films, coatings and reinforcing materials.

TEM studies: TEM was used to examine the nanoscale morphology of ionic liquid-treated nanocellulose and TEMPO-oxidised nanocellulose (Fig. 8). Ionic liquid-treated nanocellulose consisted of fibrillar structures with lengths of 34, 44, 54, 59, 78 and 79 nm, representing short and well-defined nanofibrils. In comparison, TEMPO-oxidised nanocellulose contained longer fibrils with lengths of 99, 103, 106, 110, 128 and 148 nm. The larger fibril dimensions are attributed to the structural changes associated with TEMPO oxidation.

Both samples exhibited high-aspect-ratio nanocellulose fibrils, although their morphology differed considerably. Ionic liquid-treated nanocellulose contained shorter fibrils with limited interconnection, whereas TEMPO-oxidised nanocellulose formed a denser network of longer fibrils. These

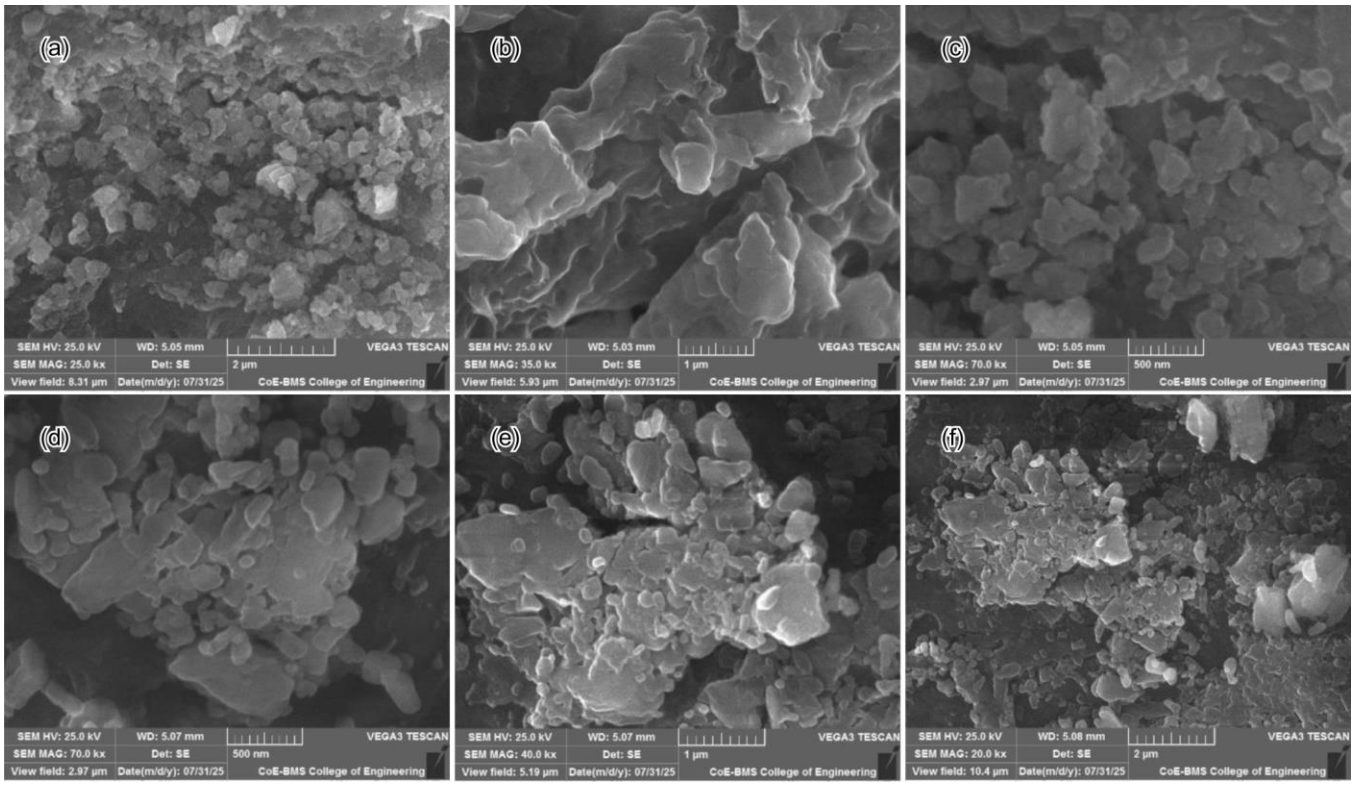

Fig. 7. SEM morphology of ionic liquid mediated nanocellulose (a, b & c) and TEMPO oxidised nanocellulose (d, e & f)

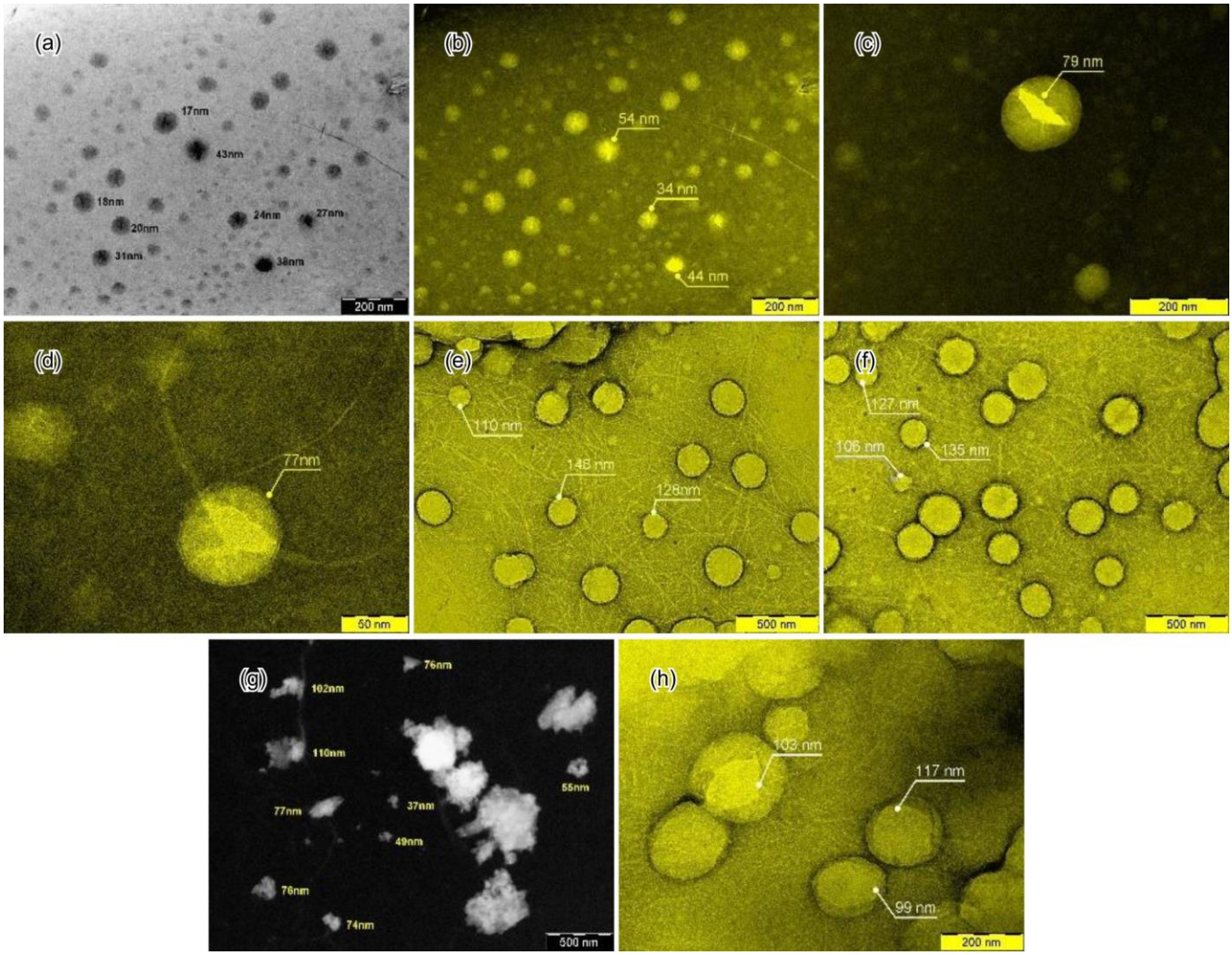

Fig. 8. TEM morphology of IL-BR-NC (a, b, c & d) and TO-BR-NC (e, f, g & h)

morphological features were comparable with those observed in the SEM micrographs and reflect the influence of the two modification methods on fibril development.

Conclusion

Banana rachis is a promising and sustainable biomass source for the production of nanocellulose through ionic liquid pretreatment and TEMPO oxidation. FTIR analysis showed that the cellulose backbone remained intact after chemical modification, while the appearance of oxygen-containing functional groups in TEMPO-oxidised nanocellulose confirmed successful surface oxidation. XRD analysis demonstrated that both treatments preserved the crystalline nature of cellulose. The crystallinity indices increased from 87.04% for native cellulose to 95.24% for ionic liquid-treated nanocellulose and 90.96% for TEMPO-oxidized nanocellulose, accompanied by rearrangement of the cellulose chains and a reduction in the amorphous regions. TGA and DTA analyses identified multi-step thermal degradation, with TEMPO-oxidized nanocellulose exhibiting higher thermal stability and greater residual char than ionic liquid-treated nanocellulose. SEM and TEM analyses showed well-developed nanofibrillar structures in both samples. Ionic liquid-treated nanocellulose consisted of shorter interconnected porous fibrils, whereas TEMPO-oxidised nanocellulose contained longer fibrils with a higher aspect ratio. These findings demonstrate that ionic liquid pre-treatment and TEMPO oxidation provide effective routes for producing nanocellulose with improved structural and thermal properties.

ACKNOWLEDGEMENTS

The authors express their sincere gratitude to their respective institutes for providing the necessary research facilities and support to carry out this research.

CONFLICT OF INTEREST

The authors declare that there is no conflict of interests regarding the publication of this article.

DECLARATION OF AI-ASSISTED TECHNOLOGIES

During the preparation of this manuscript, the authors used an AI-assisted tool(s) to improve the language and no data, results or scientific conclusions were generated by AI.

All analyses, interpretations and conclusions are the authors' own. The authors reviewed and edited the content and take full responsibility for the published work.

REFERENCES

1. R. Zuluaga, J.L. Putaux, J. Cruz, J. Vélez, I. Mondragon and P. Gañán, *Carbohydr. Polym.*, **76**, 51 (2009); https://doi.org/10.1016/j.carbpol.2008.09.024
2. J. Parameswaranpillai, J.A. Gopi, S. Radoor, C.D. Midhun Dominic, S. Krishnasamy, K. Deshmukh, N. Hameed, N.V. Salim and N. Sienkiewicz, *Composites C*, **10**, 100333 (2023); https://doi.org/10.1016/j.jcomc.2022.100333
3. A. Lahiri, S. Daniel, R. Kanthapazham, R. Vanaraj, A. Thambidurai and L.S. Peter, *J. Hazard. Mater. Adv.*, **10**, 100266 (2023); https://doi.org/10.1016/j.hazadv.2023.100266
4. F.S. Arockiasamy, B. Manoharan, V.M. Santhi, K. Prakalathan, D. Periasamy, A. Dhandapani, V. Natarajan, S. Krishnasamy, S.M.K. Thiagamani and R.A. Ilyasi, *Heliyon*, **11**, e41188 (2025); https://doi.org/10.1016/j.heliyon.2024.e41188
5. G.H. P.R. Onkarappa, H.S. Radha, V. Nikhileshwar, S.V. Betageri, *Karnatak Univ. J. Sci.*, **1**, 1 (2021).
6. H.S. Onkarappa, G.K. Prakash, G.H. Pujar, C.R. Rajith Kumar, V. Radha, M.S. Latha and V.S. Betageri, *Adv. Nat. Sci. Nanosci. Nanotechnol.*, **11**, 035001 (2020); https://doi.org/10.1088/2043-6254/ab9d23
7. T. Abitbol, A. Rivkin, Y. Cao, E. Nevo, V. Abraham, T. Ben-Shalom, S. Lapidot and O. Shoseyov, *Curr. Opin. Biotechnol.*, **39**, 76 (2016); https://doi.org/10.1016/j.copbio.2016.01.002
8. Y. Xiao, Y. Liu, X. Wang, M. Li, H. Lei and H. Xu, *Int. J. Biol. Macromol.*, **140**, 225 (2019); https://doi.org/10.1016/j.ijbiomac.2019.08.160
9. N.M. Park, S. Choi, J.E. Oh and D.Y. Hwang, *Carbohydr. Polym.*, **223**, 115114 (2019); https://doi.org/10.1016/j.carbpol.2019.115114
10. R. Mu, X. Hong, Y. Ni, Y. Li, J. Pang, Q. Wang, J. Xiao and Y. Zheng, *Trends Food Sci. Technol.*, **93**, 136 (2019); https://doi.org/10.1016/j.tifs.2019.09.013
11. D.R. Shankaran, in eds.: S. M. Bhagyaraj, O. S. Oluwafemi, N. Kalarikkal, and S. Thomas, Cellulose Nanocrystals for Health Care Applications; In: Applications of Nanomaterials, Advances and Key Technologies, Elsevier Ltd., Chap. 14, pp. 415-459 (2018); https://doi.org/10.1016/B978-0-08-101971-9.00015-6
12. F. Rol, M.N. Belgacem, A. Gandini and J. Bras, *Prog. Polym. Sci.*, **88**, 241 (2019); https://doi.org/10.1016/j.progpolymsci.2018.09.002
13. K.Y. Lee, Y. Aitomäki, L.A. Berglund, K. Oksman and A. Bismarck, *Compos. Sci. Technol.*, **105**, 15 (2014); https://doi.org/10.1016/j.compscitech.2014.08.032
14. S. An, B. Jeon, J. H. Bae, I. S. Kim, K. Paeng, M. Kim and H. Lee, *Carbohydr. Polym.*, **226**, 115259 (2019); https://doi.org/10.1016/j.carbpol.2019.115259
15. A.F. Jozala, L.C. de Lencastre-Novaes, A.M. Lopes, V. de Carvalho Santos-Ebinuma, P.G. Mazzola, A. Pessoa Jr., D. Grotto, M. Gerenutti and M.V. Chaud, *Appl. Microbiol. Biotechnol.*, **100**, 2063 (2016); https://doi.org/10.1007/s00253-015-7243-4
16. I.F. Almeida, T. Pereira, N.H.C.S. Silva, F.P. Gomes, A.J.D. Silvestre, C.S.R. Freire, J.M. Sousa Lobo and P.C. Costa, *Eur. J. Pharm. Biopharm.*, **86**, 332 (2014); https://doi.org/10.1016/j.ejpb.2013.08.008
17. I. Sulaeva, U. Henniges, T. Rosenau and A. Potthast, *Biotechnol. Adv.*, **33**, 1547 (2015); https://doi.org/10.1016/j.biotechadv.2015.07.009
18. D.Y. Hoo, Z.L. Low, D.Y.S. Low, S.Y. Tang, S. Manickam, K.W. Tan and Z.H. Ban, *Ultrason. Sonochem.*, **90**, 106176 (2022); https://doi.org/10.1016/j.ultsonch.2022.106176
19. J. Wang, J. Xu, S. Zhu, Q. Wu, J. Li, Y. Gao, B. Wang, J. Li, W. Gao, J. Zeng, and K. Chen, *Carbohydr. Polym.*, **251**, 117094 (2021); https://doi.org/10.1016/j.carbpol.2020.117094
20. W. Han, H. Xu, F. Qiu, J. Liu, H. Gu and Z. Xue, *RSC Adv.*, **15**, 2554 (2025); https://doi.org/10.1039/D4RA08079C
21. H. Yu, J. Hou, R. Basiri Namin, Y. Ni, S. Liu, S. Yu, Y. Liu, Q. Wu and S. Nie, *Carbon*, **173**, 800 (2021); https://doi.org/10.1016/J.CARBON.2020.11.069
22. C.C. Piras, S. Fernández-Prieto and W.M. De Borggraeve, *Nanoscale Adv.*, **1**, 937 (2019); https://doi.org/10.1039/C8NA00238J
23. H.S. Onkarappa, G.K. Prakash, G.H. Pujar, C.R. Rajith Kumar, V. Radha and V.S. Betageri, *Polym. Compos.*, **41**, 3153 (2020); https://doi.org/10.1002/pc.25606
24. M. Rajanna, L.M. Shivashankar, O.H. Shivamurthy, R.H.L. Shetty, S.U. Ramachandrappa, V.S. Betageri, C. Shivamallu, S. Kumar, R.G. Amachawadi and S.P. Kollur, *Polymers*, **14**, 4383 (2022); https://doi.org/10.3390/polym14204383
25. A. Isogai, T. Saito, I. Shibata, M. Yanagisawa, T. Yamamoto, Y. Koga and H. Kitaoka, *Appita Annu. Conf.*, **2**, 237 (2005).
26. C.F. Huang, C.W. Tu, R.H. Lee, C.H. Yang, W.C. Hung and K.Y. Andrew Lin, *Polym. Degrad. Stab.*, **161**, 206 (2019); https://doi.org/10.1016/j.polymdegradstab.2019.01.023
27. F. Jiang and Y. Lo Hsieh, *J. Mater. Chem. A*, **2**, 350 (2014); https://doi.org/10.1039/C3TA13629A
28. T. Sultana, H. Van Hai, C. Abueva, H.J. Kang, S.Y. Lee and B.T. Lee, *Mater. Sci. Eng. C*, **102**, 12 (2019); https://doi.org/10.1016/j.msec.2019.03.110
29. H.K. Pradeep, D.H. Patel, S. Sahana, N. Abhishek, H. Jeevan, V. Karthik, K.V. Tejasvini and D.V. Pattanashetty, *Asian J. Chem.*, **37**, 145 (2025); https://doi.org/10.14233/ajchem.2025.32878
30. C. Vilela, N. Sousa, R.J.B. Pinto, A.J.D. Silvestre, F.M.L. Figueiredo and C.S.R. Freire, *Biomass Bioenergy*, **100**, 116 (2017); https://doi.org/10.1016/j.biombioe.2017.03.016
31. D. Fang, J. Cheng, K. Gong, Q.R. Shi, X.L. Zhou and Z.L. Liu, *J. Fluor. Chem.*, **129**, 108 (2008); https://doi.org/10.1016/j.jfluchem.2007.09.004
32. R.P. Swatloski, S.K. Spear, J.D. Holbrey and R.D. Rogers, *J. Am. Chem. Soc.*, **124**, 4974 (2002); https://doi.org/10.1021/ja025790m
33. P.H. Keshavamurthysetty and D.H. Patel, *Indian J. Pharm. Educ. Res.*, **57**, S32 (2023); https://doi.org/10.5530/ijper.57.1s.5
34. C. Zinge and B. Kandasubramanian, *Eur. Polym. J.*, **133**, 109758 (2020); https://doi.org/10.1016/j.eurpolymj.2020.109758
35. S. Naduparambath, T.V. Jinitha, V. Shaniba, M.P. Sreejith, A.K. Balan and E. Purushothaman, *Carbohydr. Polym.*, **180**, 13 (2018); https://doi.org/10.1016/j.carbpol.2017.09.088
36. P. Phanthong, P. Reubroycharoen, X. Hao, G. Xu, A. Abudula and G. Guan, *Carbon Resour. Convers.*, **1**, 32 (2018); https://doi.org/10.1016/j.crcon.2018.05.004
37. H. Xue, Y. Zhang, Z. Zhao, H. Gao, W. Bao, J. Li, Z. Zhang, Q. Wang and Q. He, *J. Polym. Mater.*, **42**, 379 (2025); https://doi.org/10.32604/JPM.2025.066695
38. P. Siqueira, É. Siqueira, A.E. De Lima, G. Siqueira, A.D. Pinzón-Garcia, A.P. Lopes, M.E. Cortés Segura, A. Isaac, F.V. Pereira and V.R. Botaro, *Nanomaterials*, **9**, 78 (2019); https://doi.org/10.3390/nano9010078
39. F. Lin, Y. You, X. Yang, X. Jiang, Q. Lu, T. Wang, B. Huang and B. Lu, *Cellulose*, **24**, 5025 (2017); https://doi.org/10.1007/s10570-017-1473-9
40. H.K. Pradeep and D.H. Patel, *Asian J. Chem.*, **36**, 2079 (2024); https://doi.org/10.14233/ajchem.2024.32127